Ice Accretion Prediction on Wind Turbines and Consequent Power Losses

Ice Accretion Prediction on Wind Turbines and Consequent Power Losses

Ozcan Yirtici[1], Ismail H. Tuncer[2], Serkan Ozgen[2]

[1]Graduate Research Assistant, Dept. of Aerospace Engineering, METU, 06800 Ankara Turkey
[2]Professor, Dept. of Aerospace Engineering, METU, 06800 Ankara Turkey

E-mail: oyirtici@ae.metu.edu.tr

Abstract. Ice accretion on wind turbine blades modifies the sectional profiles and causes alteration in the aerodynamic characteristic of the blades. The objective of this study is to determine performance losses on wind turbines due to the formation of ice in cold climate regions and mountainous areas where wind energy resources are found. In this study, the Blade Element Momentum method is employed together with an ice accretion prediction tool in order to estimate the ice build-up on wind turbine blades and the energy production for iced and clean blades. The predicted ice shapes of the various airfoil profiles are validated with the experimental data and it is shown that the tool developed is promising to be used in the prediction of power production losses of wind turbines.

1. Introduction

In cold climate regions and highlands, wind turbines may be exposed to heavy atmospheric icing conditions during winter operations. In atmospheric icing conditions either clouds or supercooled fog can emerge at lower elevations with a strong temperature inversion and such conditions may last for days even weeks [1]. Ice accretion on blades result in power loss, changing blade aerodynamic characteristics and creates instrument or controller errors on wind turbines. For wind turbines in cold climate regions, icing can result in up to 17 % loss in Annual Energy Production (AEP) and reduce the power coefficient in the range of 20-50 % [2, 3]. Although an AEP loss as high as 23 % (reduction from 986 MWh to 785 MWh) based on the measured data at the Alpine Test Site Gütsch is reported, Barber et al. [4] explain this large loss by including the high turbulence and the wind gust related losses as an additional factor into the icing losses. Power curve of the Gütsch turbine is shown in Figure 1.

The amount of wind power loss depends on the amount of ice accumulation on the blades, blade design and turbine control. As in the case of the aircraft icing, Anti/De icing systems (ADIS) can be used in the wind turbines to prevent or mitigate icing. Anti-icing methods aim at preventing ice accretion (e.g. hydrophobic coating with black painting), while de-icing techniques work by removing accreted ice (e.g. heating). System power requirements and the blade rotation make the implementation of ADIS systems on wind turbines more difficult than air vehicles [5]. A critical review study about ADIS usage in wind turbines is undertaken by Parent and Ilinca [6]. Electro-thermal and hot air flow systems are generally used in the ADIS, hence wind turbines need more power to operate. Icing simulations can help in the positioning of ADIS for reducing energy consumption necessitated to operate these devices. In order to

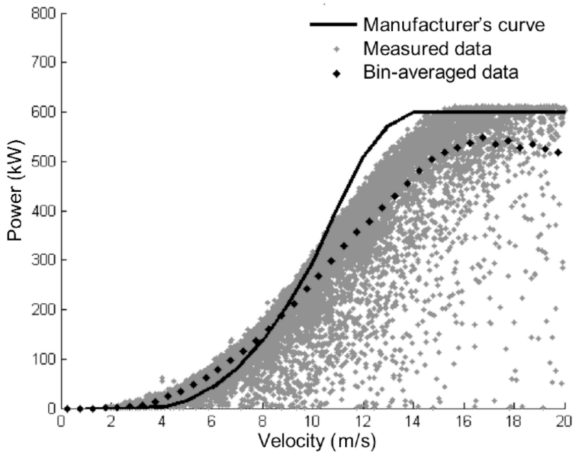

Figure 1. Power measurements at Gütsch and the bin-averaged power curve compared to the manufacturer's power curve [4].

maximize energy production from the turbine that operates under icing conditions, performance losses need to be predicted. During turbine blade design phase, a flow simulation that predicts the ice formation under icing conditions can help maintain safety, reduce the performance losses and decrease the weight.

It is well-known that icing is formed when supercooled droplets impinge on any kind of surface such as a turbine blade. Temperature, liquid water content, droplet size and surface size are basic factors affecting icing. Temperature influences the type and intensity of ice. Liquid water content determines the severity of icing, type and shape. Droplet size indicates the type and rate of icing. Surface size of iced-up body determines the rate of ice accretion. Droplets may freeze instantly and form rime ice on the surface or run downstream and freeze later forming glaze ice. Rime, glaze and mixed ice are three types of ice formation seen in atmospheric conditions. Rime ice typically forms at temperatures from 0 °C down to -40 °C. This kind of ice has a milky, opaque appearance with smooth shapes, tends to grow into the air-stream, and can be easily removed by de-icing or prevented by anti-icing systems. It usually occurs at low airspeed, low temperature and low liquid water content. Rime ice accreted turbine blade is shown in Figure 2. Glaze ice occurs at temperatures between 0 and -6 °C. Glaze ice has a transparent appearance with irregular shapes like horns and is hard to remove by de-icing systems. It occurs at high airspeed, high temperature and high liquid water content when a fraction of the water droplets freeze upon impact while remaining droplets run along the surface and freeze downstream. Because of the variation in the sectional velocity and angle of attack along the span of the wind turbine rotor, it is possible for both rime and glaze ice to be formed simultaneously.

In this study, a 2-D ice accretion prediction tool [9] is used to predict the ice formation on the turbine blade sections under given atmospheric icing conditions and flow conditions. Performance analysis of the wind turbine is then made based on the Blade Element Momentum (BEM) methodology. In BEM methodology the 2-D flow fields and the sectional aerodynamic loads at a number of sections along the blade span are considered for the estimation of the torque and the power generation of a blade. The power production losses are assessed by comparing the power generation of the clean and iced blades.

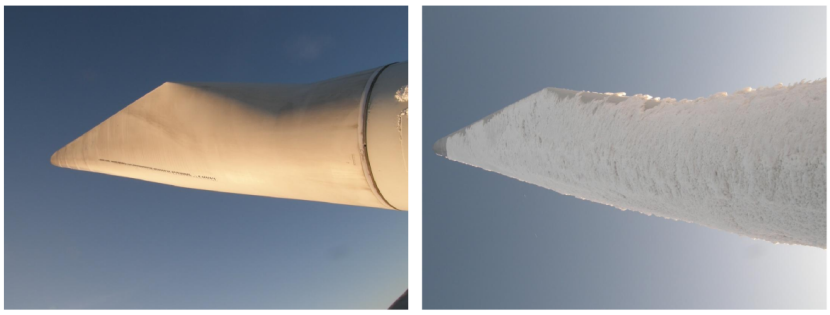

Figure 2. Clean and iced turbine blade [7].

2. Method

2.1. Ice Accretion Prediction

Ice accretion prediction involves complex physics comprising aerodynamics, heat transfer and multiphase flow, which are all time-dependent and involve geometric deformation. The numerical method employed here iteratively predicts the ice accretion on blade surfaces as a result of water droplets hitting a surface. It employs the general methodology for simulation of ice accretion on airfoils which is based on successive calculation of air flow, water droplet trajectories, collection efficiency, heat transfer balance and accreted ice. In order to determine the flow velocity field for the droplet trajectory calculations, a Hess-Smith panel method is used. Droplet trajectories are computed by using a Langrangian approach to obtain the collection efficiency distribution around the airfoil. To determine the thickness of the ice, convective heat transfer coefficients are determined by using the two-dimensional Integral Boundary Layer equation and the thermodynamic balance is achieved using the Extended Messinger model. Extended Messinger model is governed by four equations; energy equations in ice and water layers, a mass balance and a phase change or Stefan condition at the ice/water interface [8].

$$\frac{\partial T}{\partial t} = \frac{k_i}{\rho_i C p_i} \frac{\partial^2 T}{\partial y^2} \tag{1}$$

$$\frac{\partial \theta}{\partial t} = \frac{k_w}{\rho_w C p_w} \frac{\partial^2 \theta}{\partial y^2} \tag{2}$$

$$\rho_i \frac{\partial B}{\partial t} + \rho_w \frac{\partial h}{\partial t} = \rho_a \beta V_\infty \tag{3}$$

$$\rho_i L_F \frac{\partial B}{\partial t} = k_i \frac{\partial T}{\partial y} - k_w \frac{\partial \theta}{\partial y} \tag{4}$$

where θ and T are the temperatures, k_i and k_w are thermal conductivities, Cp_i and Cp_w are the specific heats and h and B are the thickness of water and ice layers, respectively. In equation 3, $\rho_a \beta V_\infty$ is impinging water mass flow rate for a panel, respectively. Meanwhile, ρ_i and L_F refer to the density of ice and the latent heat of solidification of water. In order to determine the ice and water thicknesses together with the temperature distribution at each layer, boundary and initial conditions must be specified. These are based on the following assumptions :

- Ice is in perfect contact with the airfoil surface, which is taken to be equal to the air temperature, T_a :

$$T(0, t) = T_s \tag{5}$$

- The temperature is continuous at the ice/water boundary and is equal to the freezing temperature:

$$T(B,t) = \theta(B,t) = T_f \tag{6}$$

- At the air/water (glaze ice) or air/ice (rime ice) interface, heat flux is determined by convection (Q_c), radiation (Q_r), latent heat release (Q_l), cooling by incoming droplets (Q_d), heat brought in by runback water (Q_{in}), evaporation (Q_e) or sublimation (Q_s), aerodynamic heating(Q_a) and kinetic energy of incoming droplets (Q_k):

$$For\ glaze\ ice: \quad -k_w \frac{\partial \theta}{\partial y} = (Q_c + Q_e + Q_d + Q_r) - (Q_a + Q_k + Q_{in}) \ \ at\ y = B + h \tag{7}$$

$$For\ rime\ ice: \quad -k_i \frac{\partial T}{\partial y} = (Q_c + Q_s + Q_d + Q_r) - (Q_a + Q_k + Q_{in} + Q_l) \ \ at\ y = B \tag{8}$$

- Airfoil surface is initially clean:

$$B = h = 0, \quad t{=}0 \tag{9}$$

Detailed information about this methodology can be found in Reference [9].

2.2. Wind Turbine Performance Analysis

The BEM methodology is used widely in wind turbine design and performance analysis due to its accuracy and ease of implementation. A computational tool is also needed to predict aerodynamic force coefficients since the BEM tool depends on sectional aerodynamic loads. In this study, the sectional aerodynamic force coefficients are evaluated by using the XFOIL flow solver. XFOIL is a potential flow solver with a boundary layer flow module for including the viscous effects at a given Reynolds number. It is an open source design and analysis tool written by M. Drela [10]. XFOIL is employed for both ice free and iced airfoil profiles.

3. Results and Discussion

In this study three icing cases are studied. In the first two cases, NACA 64618 and S809 airfoils, which are widely used in wind turbines, are chosen for the validation of the ice accretion prediction tool. The iced blade profiles are compared with the experimental and numerical data available in the literature. In the last case, the Aeolos 30 kW wind turbine performance analysis is carried out with the BEM methodology developed, and an icing related momentary power loss is analyzed at 11 m/s wind speed for the same wind turbine.

3.1. Ice Accretion Prediction Over S809 Turbine Blade

The present method is first validated against the experimental and numerical studies over S809 turbine blade with a chord length of 0.267 m performed by Han et al [11]. The Adverse Environment Rotor Test Stand (AERTS) is designed to generate an accurate icing cloud around test rotor to validate the capability of the facility to reproduce representative icing conditions for numerical simulations. In AERTS experiments 17 different ice accretion test cases are considered. The liquid water content is kept less than 1.5 g/m^3. Rime and glaze ice formations are observed. Reference [11] provides detailed information on the experiments performed.

The test cases considered in the present study are given in Table 1. The numerical results obtained are presented for one layer of ice accretion calculation including the splash and the break-up effects. In Figure 3, the predicted ice shapes are compared against the experimental data of the AERTS for case 19 at the leading edge of the blade sections. It is seen that both the present study and the Lewice predictions compare fairly well with the experimental data. Such an agreement is expected since the rime ice shapes are obtained from a simple algebraic equation.

Table 1. Atmospheric icing conditions for AERTS WT cases [11].

Variables	AERTS WT *case* 19 (rime ice)	AERTS WT case 15 (rime ice)	AERTS WT case 24 (glaze ice)
Ambient temperature, T_a	-9 °C	-9 °C	-9 °C
Free-stream velocity, V_∞	50 m/s	50 m/s	43 m/s
Liquid water content, ρ_a	0.05 g/m^3	0.08 g/m^3	0.3 g/m^3
Droplet diameter, d_p	20 μ m	20 μ m	20 μ m
Exposure time, t_{exp}	30 min	30 min	12 min
Ambient pressure, p_∞	95610 Pa	95610 Pa	95610 Pa
Angle of attack, α	8°	4°	6°
Humidity	100 %	100 %	100 %

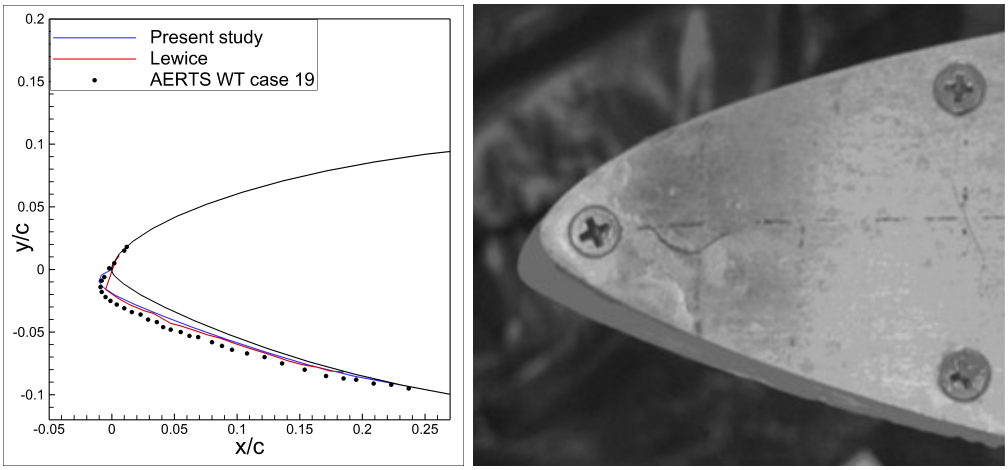

Figure 3. Predicted and experimental ice profiles on the blade for AERTS WT case 19 [11].

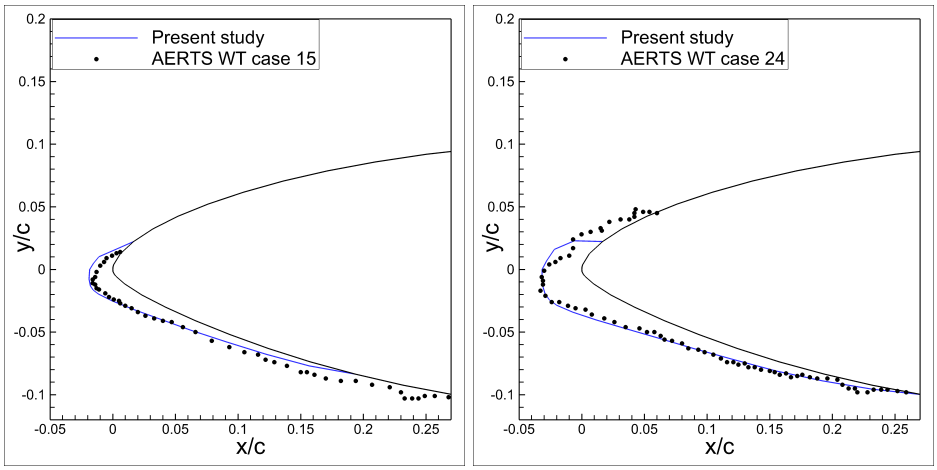

Figure 4. Predicted ice profiles for S809 airfoil for conditions in Table 1

Figure 4 shows the results and comparison with the experimental data for Case 15 and

Case 24. As seen, ice is mainly collected over the pressure side of the S809 airfoil, which is attributed to the angle of attack. The results agree reasonably well with the experimental data for both cases. The ice shape in Case 15 is in the form of rime ice because of the low liquid water content. In case 24, the extent of the iced region on the upper surface is underestimated compared to experimental data. The glaze ice shape is usually more difficult to predict, which may be attributed to the low fidelity of the runback water model.

3.2. Effect of Temperature and Droplet Size on Ice Shape

In this validation case, a 5MW pitch controlled wind turbine blade profile (NACA 64618) is used to investigate the effects of the atmospheric temperature and droplet size on the ice accretion. The geometric and flow conditions in the reference study are presented in Table 2. All simulations are performed in a single time step with splash, break up effects.

Table 2. Geometric characteristics and flow conditions used in the calculations

Airfoils	NACA 64618
Chord	1.9 m
Angle of attack	5 °
Relative air speed	25.7 m/s
Liquid water content, ρ_a	0.2 g/m^3
Droplet diameter, d_p	12, 17, 30 μ m
Ambient temperature, T_a	-2.5, -5, -7.5 °C
Exposure time, t_{exp}	120 minutes
Ambient pressure, p_∞	101300 Pa
Humidity	100 %

The results obtained are compared against the numerical study of Homola et al.[12]. In Figure 5, 6 the computed ice shapes are in agreement with those obtained numerically by Homolo et al. (Turbice). Results in Figure 5 suggest that the ice shapes for T_a = -5 °C and -7.5 °C are quite similar and exhibit rime ice characteristics. On the other hand, the ice shape obtained for T_a = -2.5 °C is typically of glaze type and is significantly different from the other two since it has a horn on the upper surface just downstream of the leading edge. These results are expected because rime ice typically occurs at low temperatures and low liquid water contents, as in this first case where T_a = -5 °C and -7.5 °C. However, T_a = -2.5 °C is a significantly high temperature in terms of ice formation and hence yields a glaze ice formation. Results in Figure 6 demonstrate that as the droplet size increases, both the ice mass and the extent of the iced region grow up. Large droplets yield higher collection efficiencies by following more ballistic trajectories. Such a condition generates a wider and a larger ice accretion as seen in Figure 6.

3.3. Power Production Losses on the Aeolos 30 kW Wind Turbine due to Icing

In the last case, the momentary power loss is investigated for a selected icing condition by comparing the local power production of the Aeolos 30 kW wind turbine for both clean and iced blades. General characteristics and operating conditions for this virtual case are given in Table 3 and geometrical properties are represented in Figure 7. The blade geometry, the sectional airfoil polar data and the test results are given in the reference [13].

Initially, the power production of the Aeolos wind turbine at various wind speeds is computed by using the BEM tool developed. In the computations 9 blade sections are employed. The power production figures obtained are compared with the test data in Figure 8. As seen, the power

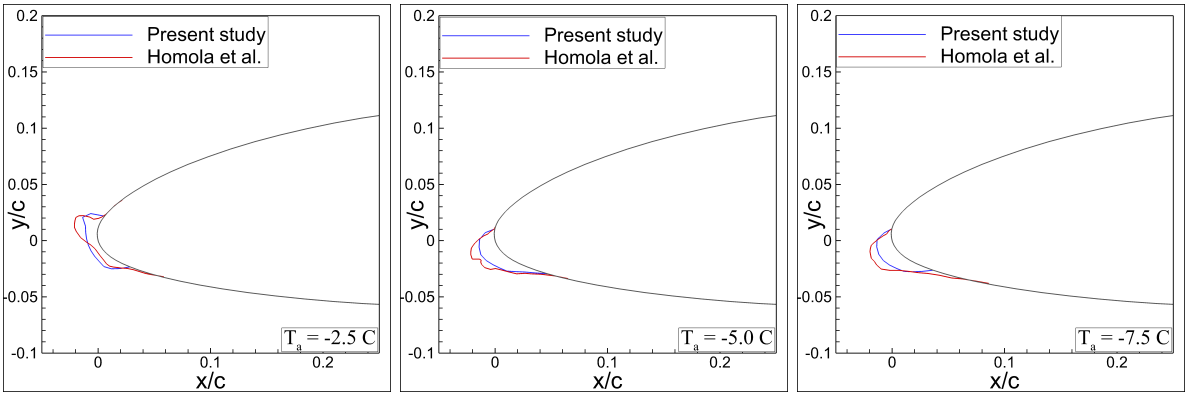

Figure 5. Predicted ice profiles for NACA 64618 airfoil for conditions in Table 2 (d_p= 17 μm)

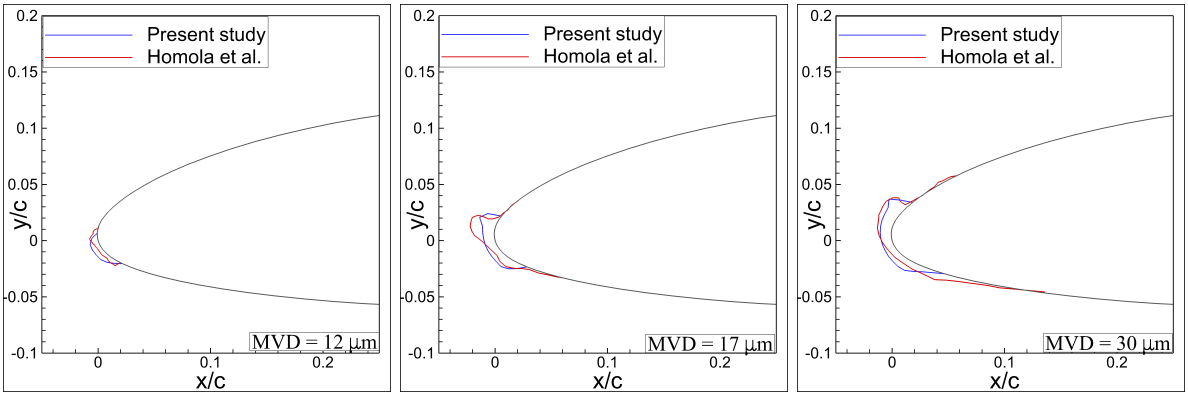

Figure 6. Predicted ice profiles for NACA 64618 airfoil for conditions in Table 2 (T_a= -2.5 °C)

Table 3. Wind turbine general characteristics and atmospheric icing conditions

Airfoils	DU93-W-210
Rotational speed	120 rpm
Root chord	0.703 m
Tip chord	0.02 m
Turbine diameter ,R	12 m
Root extension	0.5 m
Twist	17.45 degrees (max.)
Mode of power control	variable speed/yawing
Liquid water content, ρ_a	0.05 g/m^3
Droplet diameter, d_p	27 μ m
Ambient temperature, T_a	-8.0 °C
Exposure time, t_{exp}	3 hours
Ambient pressure, p_∞	95610 Pa
Humidity	100 %

productions predicted with BEM tool agree rather well with the test data. The aerodynamic loads based on the XFOIL solutions and the experimental data agree well at low wind speeds.

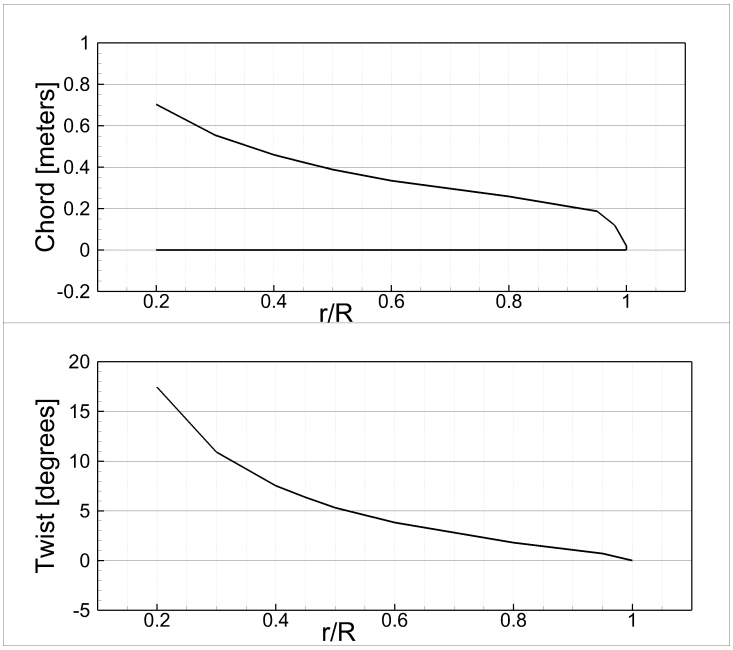

Figure 7. Blade properties of Aeolos 30 kW wind turbine.

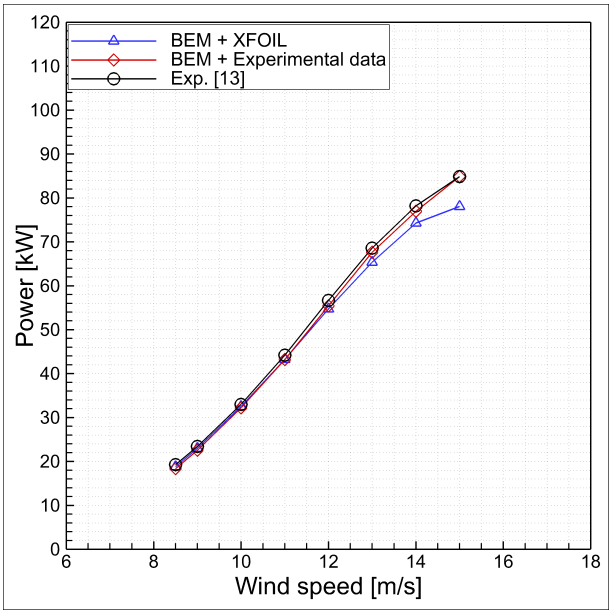

Figure 8. Power curve for Aeolos 30 kW wind turbine

At wind speeds greater than $12m/s$, the XFOIL based solution slightly underpredicts the power production. This is attributed to the empirical stall correction used at high angles of attack greater than 20 degrees encountered at high wind speeds.

Ice accretion prediction methodology developed is then used to predict the 2D ice profiles on the blade at nine different span-wise locations. Firstly, the sectional inflow velocities and the angles of attack are evaluated with the BEM method. Then, these local flow properties are used as input parameters to predict the ice shape for each blade section under the given atmospheric icing conditions.

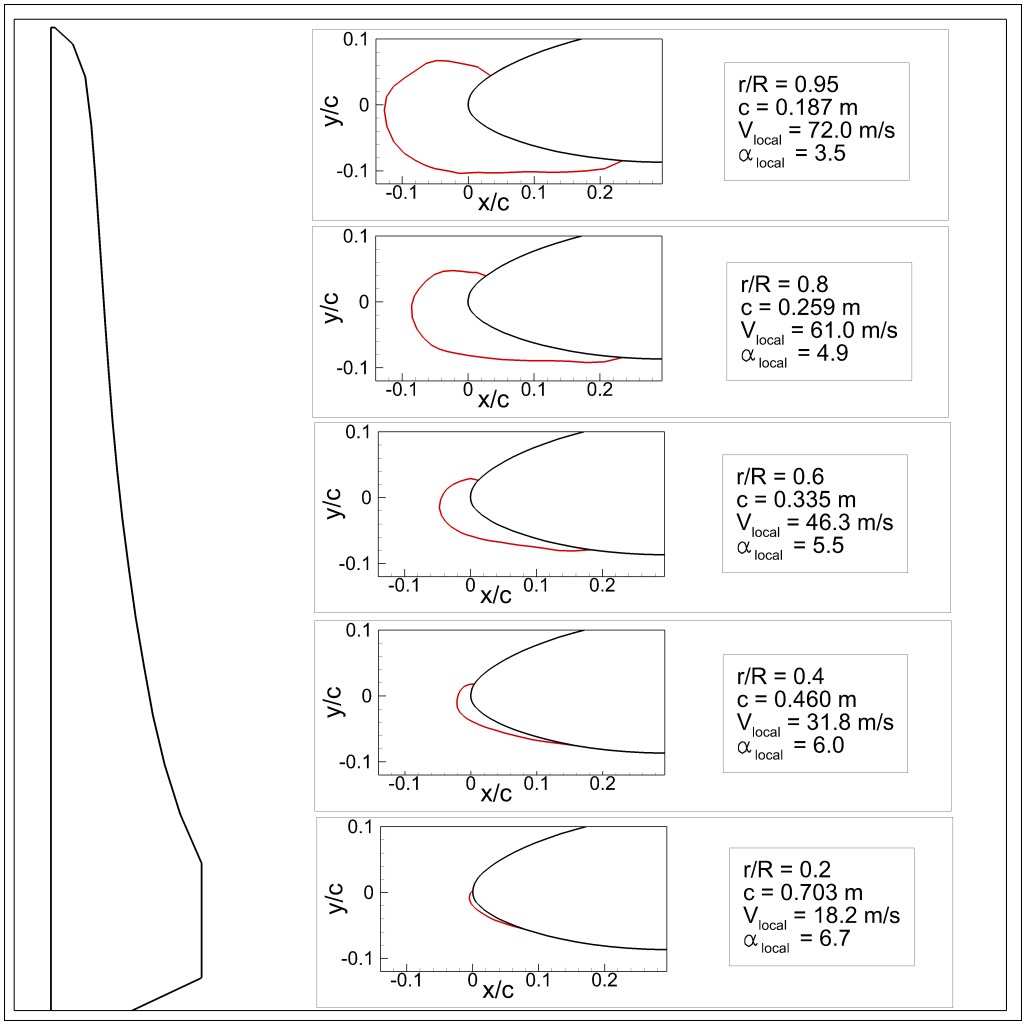

Figure 9. The Aeolos 30 kW wind turbine blade profile and predicted ice profiles along the blade span at $11m/s$ wind speed

The predicted ice profiles at five span-wise locations along the Aeolos $30kW$ wind turbine blade are given in Figure 9 for a wind speed of $11m/s$. As expected, the ice formation grows along the span due to the increasing sectional inflow velocity and the decreasing sectional chord length. It should be noted that the ice accretion significantly modifies and distorts the sectional airfoil profiles, especially near the tip section. Such a distortion degrades the aerodynamic performance of the blade. The power production for the clean and the iced blades are evaluated to be $43.78kW$ to $32.96kW$, respectively, which corresponds to a 24% momentary power loss for this icing event.

The 24% power loss prediction is in agreement with the similar studies [14, 15, 16], which are performed for various wind turbines under similar icing conditions and predict power losses in the $20-30\%$ range. It should be noted that the power loss heavily depends on the icing severity due to liquid water content, droplet diameter and icing time.

4. Conclusions

The Blade Element Momentum methodology coupled with an ice accretion prediction tool is employed to estimate energy production losses of wind turbines. The computational tool developed is first validated and then employed to predict momentary performance losses for

horizontal axis wind turbines in icing conditions. An icing event which results in 24 % power loss for the Aeolos 30 kW wind turbine is successfully simulated. It should be noted that the present study is based on 2D flow analysis. For more accurate performance predictions 3D effects should be considered.

References

[1] Fu, Ping, 2004, *Modelling and simulation of the ice accretion process on fixed or rotating cylindrical objects by the boundary element method*, *Ph. D. dissertation*, Universite du Quebec à Chicoutimi Chicoutimi.

[2] Barber S., Wang Y., Jafari Y., Chokani N. and Abhari R. S., 2011, *The impact of ice formation on wind turbine performance and aerodynamics*, *Journal of Solar Energy Engineering*, Vol.133/011007-1, February 2011.

[3] Talhaug L, Vindteknik K, Ronsten G, Horbaty R, Baring-Gould I, Lacroix A, et al., *Wind energy projects in cold climates*,1st ed. Executive Committee of the International Energy Agency Program for Research and Development on Wind Energy Conversion Systems; 2005; submitted for publication. p. 1–36, *http* : *//virtual.vtt.fi/virtual/arcticwind/reports/recommendations.pdf*, [last visited 20 April 2016].

[4] Barber S., Wang Y., Jadari S.,Chokani N., Abhari R.S., 2009, *The effect of icing on wind turbine performance and aerodynamics*, IWASIS XIII, Andermatt, Sept,2009.

[5] Fortin G. and Perron J., 2009, *Wind turbine icing and de-icing*, *47th AIAA Aerospace Sciences Meeting*

[6] Parent, O. and Ilinca, A., 2011, *Anti-icing and de-icing techniques for wind turbines: Critical review*, *Cold regions science and technology*, 65(1), pp.88-96.

[7] *Current issues on wind energy production in cold climate*, *www.nordvind.org/files/otherfiles/*0000/0084 */Current_issues_on*$_w$*ind_energy_production_in_cold_climate_ − _Wallenius.pdf*, [last visited 12 January 2016]

[8] Myers G. Tim, 2001, *Extension to the Messinger model for aircraft icing*, AIAA Journal, Vol. 39, No. 2.

[9] Özgen S. and Canıbek M., 2009, *Ice accretion simulation on multi-element airfoils using extended Messinger model.*, *Heat and Mass Transfer*, 45(3), pp.305-322.

[10] M. Drela, , *XFOIL*, *http* : *//web.mit.edu/drela/Public/web/xfoil*, [last visited on 2 June 2016]

[11] Han, Y., Palacios, J., Schmitz, S., 2012, *Scaled ice accretion experiments on a rotating wind turbine blade*, *Journal of Wind Engineering and Industrial Aerodynamics*, 109, 55-67.

[12] Homola C.M., Virk S.M.,Wallenius T., Nicklasson P.J., *Sundsbϕ* S.A, 2010, *Effect of atmospheric temperature and droplet size variation on ice accretion of wind turbine blades*, *J. Wind Eng. Ind. Aerodyn.*, doi:10.1016/j.jweia.2010.06.007

[13] *Aeolos-H 30kW - 5.5m Blade Specifications* , *http* : *//windturbinestar.com/*, [last visited on 24 May 2016]

[14] Homola M.C., Virk M.S., Nicklasson P.J. and Sundsbø P.A., 2012, *Performance losses due to ice accretion for a 5 MW wind turbine*, *Wind Energy*, 15(3), pp.379-389.

[15] Homola M.C., Nicklasson P.J., Ronsten G., 2011, *Modelling of ice induced power losses and comparison with observations*, *Proceedings of the Winterwind*, 2011.

[16] Brahimi M.T., Chocron D., Paraschivoiu I., 1997, *Prediction of ice accretion and performance degradation of HAWT in cold climates*, *AIAA Paper*, (98-0026).